PAPER • OPEN ACCESS

Dynamics and topology of non-Hermitian elastic lattices with non-local feedback control interactions

New Journal of Physics
The open access journal at the forefront of physics

Deutsche Physikalische Gesellschaft DPG
IOP Institute of Physics

Published in partnership with: Deutsche Physikalische Gesellschaft and the Institute of Physics

OPEN ACCESS

RECEIVED
10 January 2020

REVISED
1 March 2020

ACCEPTED FOR PUBLICATION
20 March 2020

PUBLISHED
1 May 2020

PAPER

Dynamics and topology of non-Hermitian elastic lattices with non-local feedback control interactions

Matheus I N Rosa[1,2,3] **and Massimo Ruzzene**[2]

[1] School of Mechanical Engineering, Georgia Institute of Technology, Atlanta GA 30332, United States of America
[2] Department of Mechanical Engineering, University of Colorado Boulder, Boulder CO 80309, United States of America
[3] Author to whom any correspondence should be addressed.

E-mail: matheus.rosa@colorado.edu

Keywords: meta materials, non-Hermitian systems, wave amplification, non-reciprocal wave propagation, topological modes

Abstract

We investigate non-Hermitian elastic lattices characterized by non-local feedback interactions. In one-dimensional lattices, proportional feedback produces non-reciprocity associated with complex dispersion relations characterized by gain and loss in opposite propagation directions. For non-local controls, such non-reciprocity occurs over multiple frequency bands characterized by opposite non-reciprocal behavior. The dispersion topology is investigated with focus on winding numbers and non-Hermitian skin effect, which manifests itself through bulk modes localized at the boundaries of finite lattices. In two-dimensional lattices, non-reciprocity is associated with directional wave amplification. Moreover, the combination of skin effect in two directions produces modes that are localized at the corners of finite two-dimensional lattices. Our results describe fundamental properties of non-Hermitian elastic lattices, and suggest new possibilities for the design of meta materials with novel functionalities related to selective wave filtering, amplification and localization. The considered non-local lattices also provide a platform for the investigation of topological phases of non-Hermitian systems.

1. Introduction

Meta materials and phononic crystals are periodic structures designed to manipulate acoustic and elastic waves [1, 2]. Potential applications include vibration attenuation [3], noise reduction [4], wave focusing [5], cloaking [6], and the design of seismic barriers [7]. Recent breakthroughs in topological insulators in solid state physics [8] and photonics [9] have motivated the search for topology-based functionalities in mechanical and acoustic meta materials. This has culminated in the consolidation of topological mechanics [10] and acoustics [11] as active research fields [12]. Topological states have been successfully observed in several platforms [13–21], and have been pursued to achieve robust, diffraction-free wave motion. Additional functionalities have been explored in the context of topological pumping [22–26], quasi-periodicity [27–29], and non-reciprocal wave propagation in active [30–36] or passive non-linear [37–40] systems. These works and the references therein illustrate a wealth of strategies for the manipulation of elastic and acoustic waves, and suggest intriguing possibilities for technological applications in acoustic devices, sensing, energy harvesting, among others.

Considerable efforts have been recently devoted towards the exploration of non-Hermiticity in various physical platforms such as in optical [41, 42], opto mechanical [43], acoustic [44], and mechanical [45, 46] systems. Non-Hermitian systems are non-conservative systems where loss and/or gain are inherently present from interactions with the environment. In this context, the realization that parity-time (PT) symmetric non-Hermitian Hamiltonians may exhibit purely real spectra [47] has sparkled renewed interest in non-Hermitian physics [48, 49]. Indeed, a large portion of recent studies has focused on PT symmetry and the role of exceptional points [50], whose intriguing properties lead to unconventional phenomena such as unidirectional invisibility [44, 51], single-mode lasers [52] and enhanced sensitivity to perturbations [53,

54]. Understanding the topological properties of non-Hermitian systems has also been the focus of many research efforts [55–59]. Initial interest revolved around exceptional points exhibiting unique topological features with no counterparts in Hermitian systems, such as Weyl exceptional rings [60], bulk Fermi arcs and half-integer topological charges [61]. Further observations of a seemingly breakdown of the bulk-boundary correspondence principle [62, 63] has led to proposals for a general classification of the topological phases of non-Hermitian systems [55, 56, 64]. A particular point of interest is the observation of the *non-Hermitian skin effect* [65–71], whereby all Eigen states of one-dimensional (1D) systems are localized at a boundary, in sharp contrast with the extend Bloch modes of Hermitian counterparts. This intriguing feature of non-Hermitian lattices has recently been experimentally demonstrated using topo electrical circuits [72] and quantum walks of single photons [73]. Further theoretical investigations have also shown higher order skin modes localized at corners and edges of 2D and 3D non-Hermitian lattices [74, 75].

While most studies have so far focused on non-Hermitian optical and condensed matter systems, a few works have explored non-Hermiticity in elastic and acoustic media, most of which focus on PT phase transitions and exceptional points [44, 76–82]. More recently, feedback control has been pursued to establish non-reciprocal interactions in a mechanical meta material that emulates the non-Hermitian Su–Schrieffer–Heeger (SSH) model [45]. Such setting was used to experimentally demonstrate the existence of zero-frequency edge states in the non-Hermitian topological phase, and also to realize unidirectional wave amplification [46]. Motivated by these notable contributions, we here investigate a family of 1D and 2D elastic lattices with non-local, proportional feedback interactions and explore a series of unconventional *phenomena* stemming from their non-Hermiticity. Starting from a wave propagation perspective, we demonstrate that the frequency bands of 1D lattices are entirely non-reciprocal, due to the presence of gain and loss in opposite propagation directions. Such behavior is tunable based on the non-locality of the feedback interactions, which can be exploited to establish multiple frequency bands with interchanging non-reciprocal behavior. We also show that the bulk Eigen modes of finite lattices are localized at a boundary according to the non-Hermitian skin effect, and that their localization edge is well predicted by the winding number of the complex dispersion bands, which is aligned with recent findings on quantum lattices [55]. Our analysis is then extended to 2D lattices where non-reciprocity manifests itself as a preferential direction for wave amplification, which is defined by the control interactions. We show that the non-local control in 2D lattices establishes multiple non-reciprocal frequency/wavenumber bands with different preferential directions of amplification. Finally, we investigate skin modes in finite lattice strips and show that their combined effect in two directions leads to modes localized at the corners of finite 2D lattices. Our work provides fundamental perspectives on a new class of non-Hermitian elastic lattices with feedback interactions and contributes to recent efforts in exploring non-Hermiticiy for the design of meta materials with novel functionalities [45, 46].

This paper is organized as follows: following this introduction, the analysis of wave propagation and topological properties of 1D lattices with feedback interactions is presented. Next, results are extended to 2D lattices where directional wave amplification and corner modes are demonstrated. Finally, we summarize the main results of the work and outline potential future research directions.

2. One-dimensional elastic lattices with feedback interactions

We consider 1D elastic lattices of equal masses m, separated by a unit distance, and connected by springs of equal stiffness k (figure 1). Control interactions are introduced by considering an additional force, applied to the nth mass, that reacts proportionally to the elongation of a spring at location $n-a$ ($a \in \mathcal{I}$). This force is expressed as $f_n = k_c(u_{n-a} - u_{n-(a+1)})$, where k_c denotes the proportional control gain, and u_n is the displacement of mass n along the x axis. In the absence of external forces, the governing equation of motion for mass n is expressed as

$$m\ddot{u}_n + 2ku_n - k(u_{n+1} + u_{n-1}) - k_c(u_{n-a} - u_{n-(a+1)}) = 0. \tag{1}$$

For a lattice of N masses, the equations of motion can be written in matrix form:

$$\mathbf{M}\ddot{\boldsymbol{u}} + \mathbf{K}\boldsymbol{u} = \mathbf{0}, \tag{2}$$

where $\boldsymbol{u} = [u_1, u_2, \ldots, u_N]^{\mathrm{T}}$, and $\mathbf{M}, \mathbf{K}$ respectively denote the mass and stiffness matrices. The lattice is non-Hermitian since the stiffness matrix $\mathbf{K}$ is real but not symmetric, i.e. $\mathbf{K}^{\mathrm{T}} \neq \mathbf{K}$. Although active components would be required for the implementation of the feedback interactions, the stiffness matrix $\mathbf{K}$ includes the additional interactions associated with k_c in equation (1). Numerical simulations are performed through standard procedures, whereby, for example, transient time domain responses can be

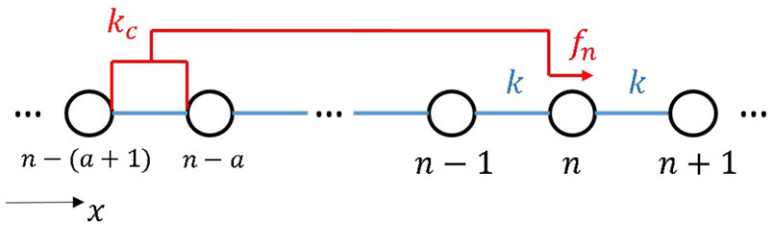

Figure 1. One-dimensional lattice of equal masses m connected by springs of stiffness k with feedback control interactions. A force $f_n = k_c(u_{n-a} - u_{n-(a+1)})$ is applied to each mass along the lattice, corresponding to a reaction proportional to the elongation of a spring a units behind.

evaluated by numerical integration of equation (2), for assigned forcing. Also, Eigen frequencies, mode shapes and dispersion properties can be obtained through the solution of Eigenvalue problems obtained by applying boundary conditions to finite lattices, or by imposing Bloch conditions on a unit cell.

2.1. Dispersion relations and non-reciprocity

We impose a Bloch-wave solution of the form $u_n = Ue^{i(\omega t-\mu n)}$, where ω and μ respectively denote angular frequency and non-dimensional wavenumber. Substitution in equation (1) yields the dispersion relation

$$\Omega^2 = 2(1-\cos\mu) - \gamma_c(1-e^{i\mu})e^{i\mu a} \tag{3}$$

where $\Omega = \omega/\omega_0$, with $\omega_0 = \sqrt{k/m}$, and $\gamma_c = k_c/k$. The feedback interaction makes the right-hand side of equation (3) generally complex, which results in complex frequencies $\Omega = \Omega_r + i\Omega_i$ that come in pairs $\{\Omega, -\Omega\}$. Without loss of generality, we focus on the solution Ω with positive real part ($\Omega_r > 0$), which corresponds to a wave $u_n = Ue^{i(\Omega_r\tau-\mu n)}e^{-\Omega_i\tau}$, ($\tau = t\omega_0$), that travels along the positive (negative) x direction when μ is positive (negative), and that is exponentially attenuated (amplified) in time when Ω_i is positive (negative).

We first investigate the case of local control ($a = 0$), i.e. with the feedback force proportional to the elongation of the left adjacent spring. Figure 2(a) displays the dispersion for $\gamma_c = 0.1$ (solid red lines), superimposed to the dispersion $\Omega = \sqrt{2(1-\cos\mu)}$ of a lattice with no feedback $\gamma_c = 0$ (dashed black lines). A remarkable feature of the dispersion lies in its imaginary component: positive wavenumbers are associated with loss due to positive Ω_i values (shaded pink areas), while negative wavenumbers are associated with gain due to negative Ω_i values (shaded green areas). Therefore, the lattice with $\gamma_c = 0.1$ amplifies waves traveling to the left and attenuates waves traveling to the right, while an opposite behavior is observed for $\gamma_c = -0.1$ (figure 2(c)). The non-reciprocity associated with gain and loss is confirmed by time domain simulations, where a 5-cycle sine burst of center frequency $\Omega = 0.3$ (figures 2(e) and (f)) is applied to the center mass of a chain of $N = 1500$ masses. The resulting transient responses are displayed in figures 2(b) and (d) in the form of waterfall plots. For visualization purposes, the displacement along the lattice for each time instant is normalized by the instantaneous L_∞ norm (along x), which is employed in the associated log-scale color map. A wave packet is amplified as it propagates to the left for $\gamma_c = 0.1$, and to the right for $\gamma_c = -0.1$. The frequency/wavenumber (2D-FT) content of the wave packets shows the displacement in reciprocal space $\hat{u}(\mu, \Omega)$:contours plots superimposed to the theoretical dispersion curves in figures 2(a) and (c) confirm the expected non-reciprocal behavior highlighted by the concentration of the spectral content of the transients in the gain (green) portions of the reciprocal space.

Next, we investigate the role of non-local interactions defined by $a > 0$ values. The dispersion for $a = 1$ and $\gamma_c = 0.1$ (figure 3(a)) features an imaginary frequency curve with two distinct regions of gain or loss for each propagation direction. The behavior is entirely non-reciprocal: positive and negative wavenumbers with the same absolute value correspond to attenuation along one direction, and amplification along the other, as highlighted by the shaded green and pink regions. In fact, one can verify in equation (3) that $\Omega_r^2(\mu) = \Omega_r^2(-\mu)$ and $\Omega_i^2(\mu) = -\Omega_i^2(-\mu)$. By using basic properties related to the square roots of a complex number (not described here for brevity), one can confirm reciprocity for the real part of the dispersion ($\Omega_r(\mu) = \Omega_r(-\mu)$), and non-reciprocity for the imaginary part ($\Omega_i(\mu) = -\Omega_i(-\mu)$). Due to this property, the amplification and attenuation wavenumber ranges defined by the imaginary part of the dispersion can be translated to the real frequency dispersion curves by matching the corresponding wavenumber intervals (figure 3(a)). The procedure highlights two non-reciprocal frequency bands; the first amplifies waves

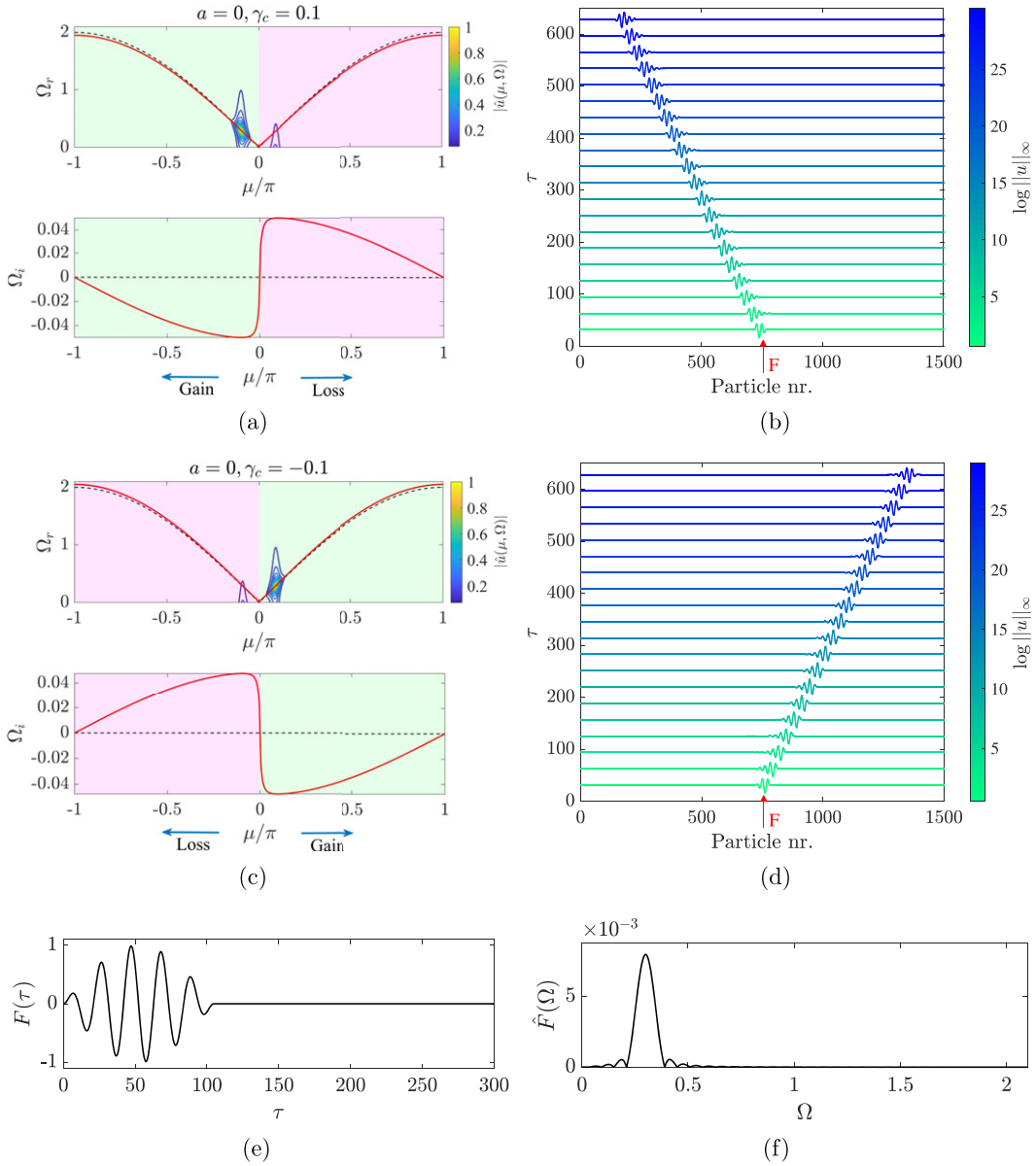

Figure 2. Non-reciprocal amplification and attenuation of waves in lattices with local feedback interactions ($a = 0$). The dispersion $\Omega(\mu)$ for $\gamma_c = 0.1$ and $\gamma_c = -0.1$ are respectively shown in (a) and (c) (solid red lines), superimposed to the dispersion of the passive lattice with $\gamma_c = 0$ (dashed black lines). Attenuation and amplification zones are identified by shaded pink and green areas revealing non-reciprocal behavior: the lattice with $\gamma_c = 0.1$ amplifies waves traveling to the left and attenuates waves traveling to the right, while $\gamma_c = -0.1$ results in a opposite behavior. Transient simulation results reported as waterfall plots in (b) and (d) illustrate the non-reciprocal behavior, which is further confirmed by their dispersion estimated through FT operations (contours in (a, c)). The force applied to mass $n = 750$ is displayed in the time and in the frequency domains in (e) and (f), respectively.

traveling to the left, while the latter amplifies waves traveling to the right. In general, when considering higher a values the number of non-reciprocal bands increases, usually being equal to $a + 1$. For example, the dispersion for $a = 3, \gamma_c = 0.1$ displayed in figure 3(c) exhibits a total of four non-reciprocal frequency bands, as highlighted by shaded green and pink regions.

Non-reciprocity with non-local feedback is confirmed by the transient time domain simulations results displayed in figures 3(b) and (d). A broad-band input signal (figures 3(e) and (f)) applied to the center mass of the lattice illustrates de-multiplexing of the input signal resulting from the amplification and propagation of one wave packet along each direction for $a = 1$ (figure 3(b)), and of two wave packets along each direction for $a = 3$ (figure 3(d)). The corresponding 2D-FTs are superimposed to the dispersion curves in figures 3(a) and (c), confirming the predicted amplification bands. We also note that amplification of wave packets is intensified around wavenumbers associated with local minima of Ω_i, corresponding to the largest time amplification exponents.

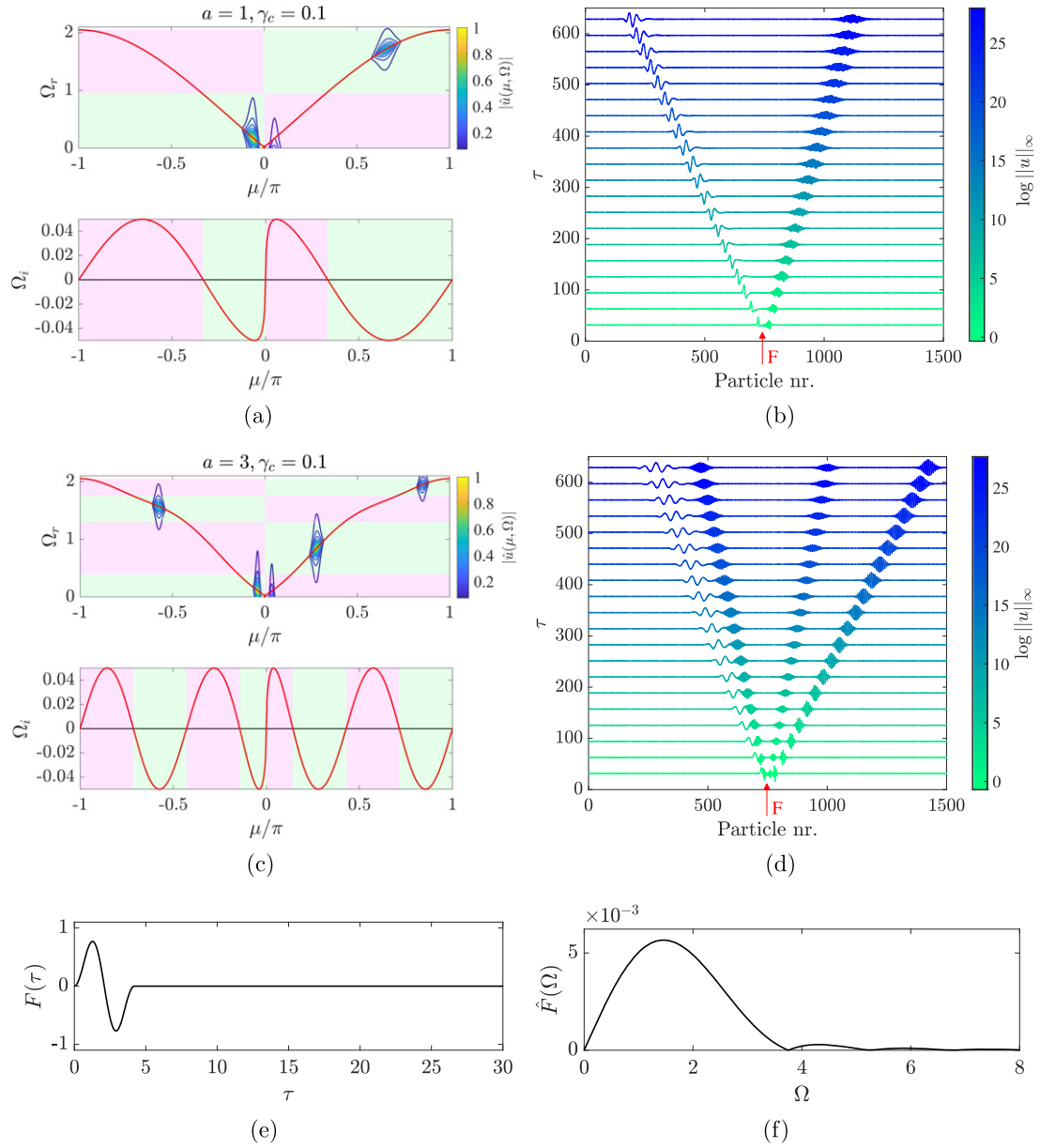

Figure 3. Non-reciprocal amplification and attenuation of waves in lattices with non-local feedback interactions ($a > 0$). The dispersion $\Omega(\mu)$ for $a = 1$ and $a = 3$ are displayed in (a) and (c), respectively. The non-local feedback interactions result in multiple frequency bands with non-reciprocity in amplification and attenuation (shaded green and pink areas). Transient time domain simulations to a broad-band input force (e, f) illustrate the non-reciprocal behavior: one wave packet is amplified and propagates along each direction in (b), while two wave packets are amplified and propagate along each direction in (d). Their dispersion (contours in (a, c)) estimated through FT operations are in good agreement with the non-reciprocal bands. The broadband input force applied to mass $n = 750$ is displayed in the time and in the frequency domains in (e) and (f), respectively.

2.2. Bulk topology and non-Hermitian skin effect

Next, we investigate the topological properties of non-Hermitian lattices and their relation to bulk modes localized at the boundaries of finite lattices. Starting with local feedback interactions ($a = 0$), figures 4(a) and (g) display the complex representation of the dispersion for $\gamma_c = 0.1$ and $\gamma_c = -0.1$, respectively, where both real and imaginary frequency components are plotted against the wavenumber μ. The projections of the dispersion bands on the complex plane in figures 4(b) and (h) reveal closed loops (red lines) parameterized by μ, with arrows denoting the direction of increasing μ. As recently demonstrated in [55], the winding number of the loops define a topological invariant associated with the localization of bulk modes for finite lattices. The winding number of a dispersion band $\Omega(\mu)$ is given by [83]

$$\nu = \frac{1}{2\pi \mathrm{i}} \int_{-\pi}^{\pi} \frac{\Omega'}{\Omega - \Omega_b} \mathrm{d}\mu, \tag{4}$$

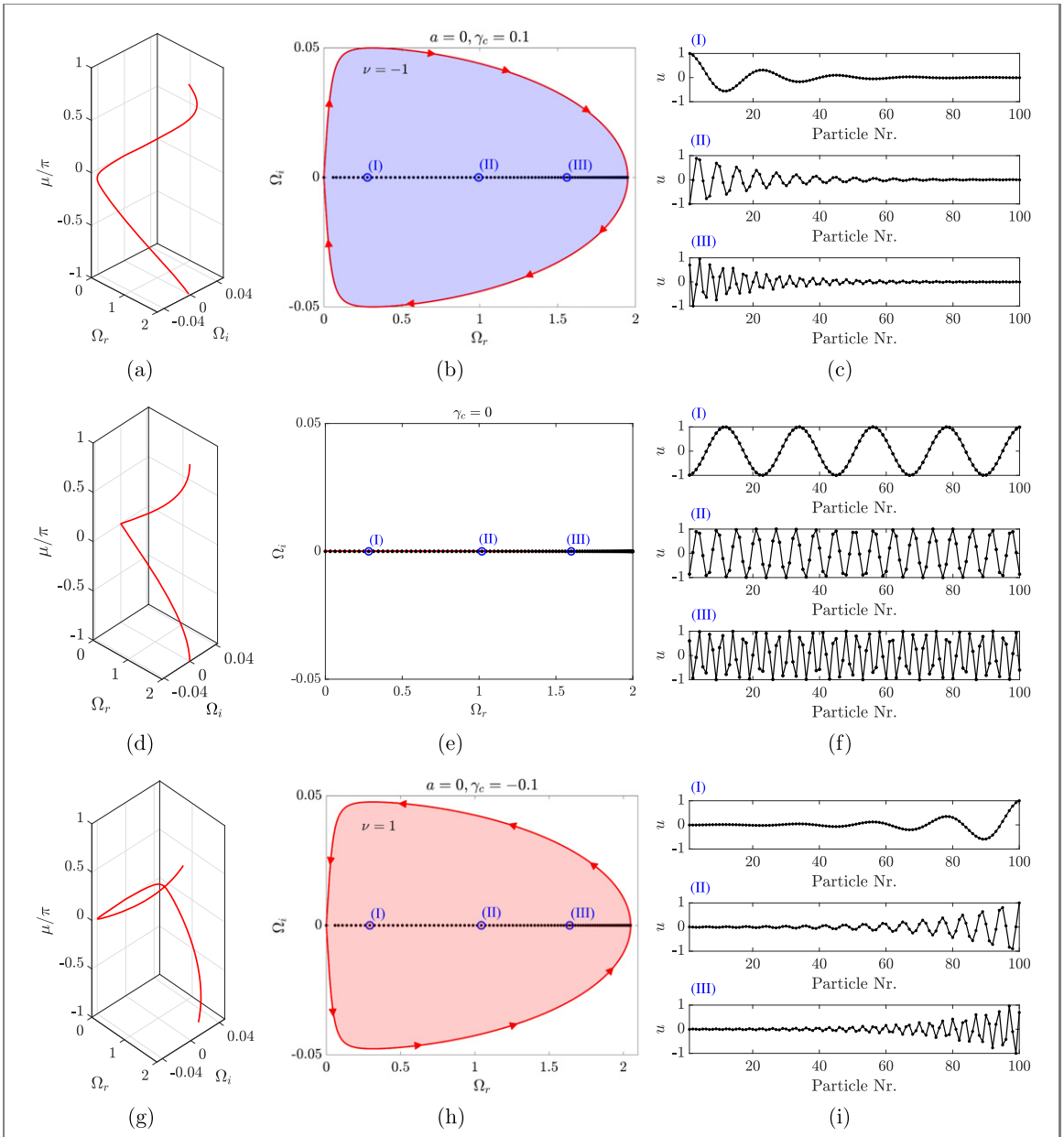

Figure 4. Dispersion topology and non-Hermitian skin effect in lattices with local feedback interactions ($a = 0$). The complex dispersion bands $\Omega(\mu)$ for lattices with $\gamma_c = 0.1$ and $\gamma_c = -0.1$ are displayed in (a) and (g), and their projection on the complex plane define closed loops as displayed in (b) and (h). Shaded blue and red areas represent regions with winding number $\nu = -1$ and $\nu = 1$, respectively. In contrast, the Hermitian lattice ($\gamma_c = 0$) exhibits a real dispersion (d), whose projection on the complex plane defines a flat band (e). Bulk modes of a finite lattice with $N = 100$ masses are localized at the left (c) or right (i) boundaries for the non-Hermitian lattices, when their Eigen frequencies (black dots in (b, h)) lie inside regions with $\nu = -1$ or $\nu = 1$, respectively. In the Hermitian case, the Eigen frequencies of the finite lattice lie on top of the flat band (black dots in (e)), and define globally spanning bulk modes (f).

where $\Omega' = \partial\Omega/\partial\mu$, and the base frequency Ω_b is an arbitrary point in the complex plane not belonging to the dispersion band [55], i.e. $\Omega_b \neq \Omega(\mu)$. Geometrically, the winding number counts the number of times the dispersion loops encircles the base frequency, and is positive for counter clockwise rotations. In the dispersion of figures 4(b) and (h), shaded blue and red areas denote regions for which any point has a winding number of $\nu = -1$ or $\nu = 1$, respectively. Their values are confirmed by numerical integration of equation (4) for a given point inside the loop, and by using the property that points inside a simply connected region have the same winding number [83], which clarifies the arbitrary nature of the base frequency Ω_b. Points outside the dispersion loops are trivially associated with a zero winding number $\nu = 0$.

Hence, the feedback control interactions define distinct phases characterized by winding numbers which exhibit opposite behaviors for lattices with $\gamma_c = 0.1$ and $\gamma_c = -0.1$. These behaviors manifest as localized bulk Eigen modes in finite lattices, a phenomenon known as *non-Hermitian skin-effect* (NHSE) [65–71]. As

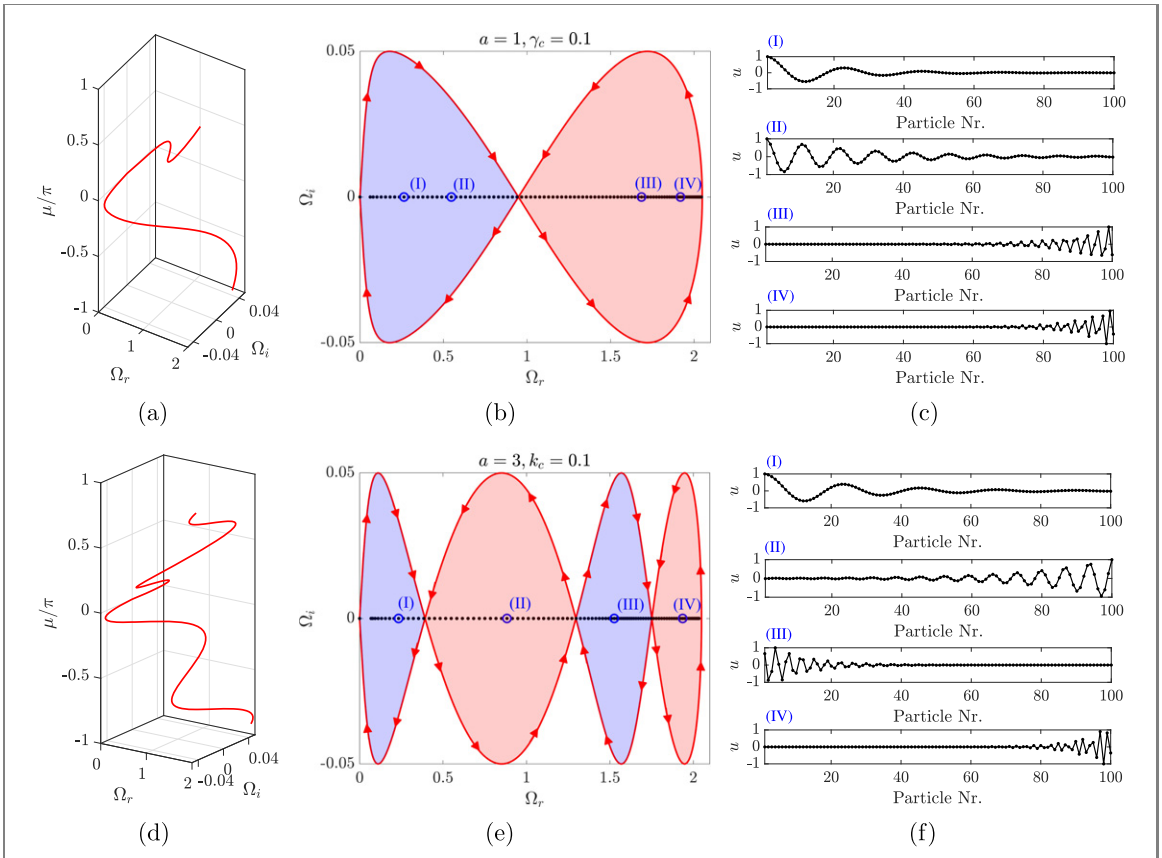

Figure 5. Dispersion topology and non-Hermitian skin effect in lattices with non-local feedback interactions ($a > 0$). The complex dispersion bands $\Omega(\mu)$ for lattices with $a = 1$ and $a = 3$ are displayed in (a) and (d). Their projection on the complex plane define the closed loops shown in (b) and (e). The non-locality of the feedback interactions result in multiple phases defined within a single band, as highlighted by shaded blue and red areas representing regions with winding number $\nu = -1$ and $\nu = 1$, respectively. Bulk modes of a finite lattice with $N = 100$ masses whose Eigen frequencies (black dots) lie inside regions with $\nu = -1$ or $\nu = 1$ are respectively localized at the left or right boundaries, as confirmed by the representative examples in (c) and (f).

an illustration, the Eigen frequencies of a finite lattice with $N = 100$ masses under free-free boundary conditions are displayed as black dots in figures 4(b) and (h), while representative Eigen modes marked by the blue circles are displayed in figures 4(c) and (i). Aligned with recent findings in quantum lattices [55], our results show that Eigen frequencies belonging to regions with $\nu < 0$ define bulk modes localized at the left boundary (figure 4(c)), while $\nu > 0$ values produce localization at the right boundary (figure 4(f)). This behavior is also in agreement with the non-reciprocal wave properties reported in figure 2: the phase with $\nu = -1$ is related to waves amplified to the left and attenuated to the right, hence the modes of a finite lattice are localized at the left boundary, while the opposite holds true for $\nu = 1$. In contrast, the Hermitian lattice ($\gamma_c = 0$) exhibits a real dispersion band (figure 4(d)), whose projection on the complex plane defines a band with zero imaginary component (figure 4(e)). The Eigen frequencies of a finite Hermitian lattice discretely sample the band (black dots in figure 4(e)), and define globally spanning bulk modes (figure 4(f)). The topology of the Hermitian lattice is trivial, since its dispersion does not form a closed loop in the complex plane. Indeed, in Hermitian systems, edge states can only be found for frequencies inside a band-gap [18, 22, 29], with the localization of bulk modes at the boundaries due to NHSE is a feature unique to non-Hermitian systems.

The dispersion topology for non-local lattices ($a > 0$) is characterized by multiple phases within a single band. Figures 5(a) and (b) displays the dispersion $\Omega(\mu)$ for $\gamma_c = 0.1$ and $a = 1$, while results for $a = 3$ are reported in figures 5(d) and (e). The dispersion loops feature multiple regions with interchanging winding numbers: the lattice with $a = 1$ is characterized by two phases, while the lattice with $a = 3$ is characterized by four phases, as highlighted by shaded blue and red areas denoting regions with $\nu = 1$ and $\nu = -1$. Bulk modes of finite lattices (black dots) are localized at the left or the right boundary (figures 5(c) and (f)) when corresponding Eigen frequencies lie inside regions with $\nu = -1$ and $\nu = 1$, respectively. We remark that, although free–free boundary conditions are used throughout this paper, the NHSE also occurs under different boundary conditions, such as fixed–fixed or fixed–free, and the localization edges are always

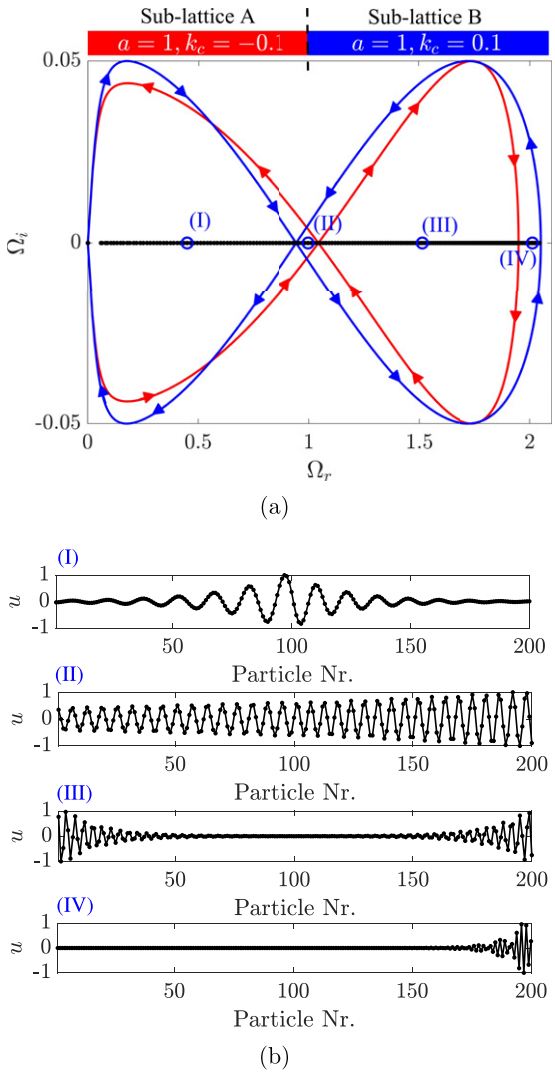

Figure 6. Bulk properties of finite lattice in a domain-wall configuration. Red and blue loops in (a) represent the dispersion of sub-lattices A and B, respectively, while black dots correspond to the Eigen frequencies of the finite lattice with $N = 200$ masses. The localization properties of the representative modes displayed in (b) are interpreted based on where their Eigen frequencies lie in the complex plane. In the first region the effects of $\nu = 1$ for sub-lattice A and $\nu = -1$ for sub-lattice B lead to bulk modes localized at the interface (mode I). In the second large region, modes are localized at both edges (mode III) since $\nu = -1$ for sub-lattice A and $\nu = 1$ for sub-lattice B. Mode II lies in a region with $\nu = 1$ for both sub-lattices and exhibits a slight tendency of amplification towards the right boundary, while mode IV lies outside the dispersion loop of sub-lattice A and inside a region with $\nu = 1$ for sub-lattice B, resulting in localization at the right boundary.

correctly predicted based on the winding number of the complex dispersion bands. Two examples for the lattice with $a = 3$ with different boundary conditions are presented in the appendix.

The characterization of bulk properties through winding numbers can also be applied to systems coupled by a domain wall, which leads to the existence of bulk interface modes and of 'double skin modes' (modes localized at both boundaries). We illustrate this by considering a finite lattice of $N = 200$ masses, where the first 100 masses are characterized by $a = 1, \gamma_c = -0.1$ (sub-lattice A), and the second half by $a = 1, \gamma_c = 0.1$ (sub-lattice B). The spectral properties of the coupled system in figure 6(a), where the red loop denotes the dispersion of sub-lattice A, while the blue loop that of sub-lattice B. Also, black dots are the Eigen frequencies of the finite lattice, while a few selected modes marked by blue circles have their mode shapes displayed in figure 6(b). The modes inside the first region (represented by mode I in figure 6(b)) are localized at the interface, since in that region $\nu = 1$ for sub-lattice A implies a tendency of localization towards its right, while $\nu = -1$ for sub-lattice B implies a tendency for localization towards its left. Modes inside a second large region (represented by mode III in figure 6(b)) exhibit an opposite behavior: $\nu = -1$ for sub-lattice A implies a tendency for localization to its left, while $\nu = 1$ for sub-lattice B implies a tendency to right localization. These modes are therefore 'double skin modes' simultaneously localized at both boundaries. In a small region between the two larger regions, the modes are associated with $\nu = 1$ for both sub-lattices, and a slight tendency of amplification towards the right boundary is observed (mode II).

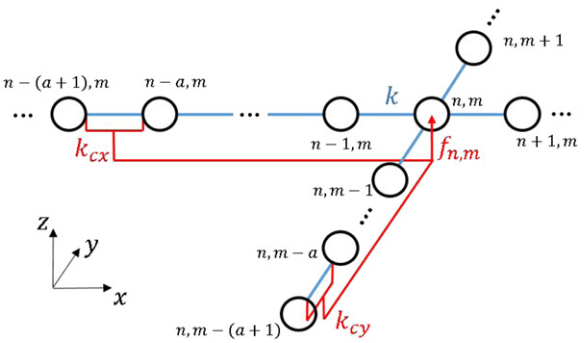

Figure 7. Two-dimensional lattice of equal masses m connected by springs of stiffness k with feedback control interactions. A force $f_{n,m} = k_{c_x}(u_{n-a,m} - u_{n-(a+1),m}) + k_{c_y}(u_{n,m-a} - u_{n,m-(a+1)})$ is applied to each mass in the lattice, corresponding to a reaction proportional to the elongation of springs a units behind in the x direction, and a units below in the y direction.

A final set of modes represented by mode IV lie outside the dispersion loop for sub-lattice A, and in a region with $\nu = 1$ for sub-lattice B, which results in localization to the right.

3. Two-dimensional elastic lattices with feedback interactions

We now extend the study to 2D lattices consisting of equal masses m connected by springs k, separated by a unit distance in both x and y directions. Each mass moves along the perpendicular z direction (figure 7), so that the springs react with a force proportional to the relative vertical motion of neighboring masses. Feedback interactions are defined by an additional force applied to mass n, m proportional to the elongation of a spring a units behind in the x and y directions. This force is expressed as $f_{n,m} = k_{c_x}(u_{n-a,m} - u_{n-(a+1),m}) + k_{c_y}(u_{n,m-a} - u_{n,m-(a+1)})$, where k_{c_x} and k_{c_y} are the proportionality constants for elongations of springs aligned with the x and y directions, respectively. The governing equation of motion in the absence of external forces is

$$\begin{aligned} m\ddot{u}_{n,m} + 4ku_{n,m} - k(u_{n-1,m} + u_{n+1,m} + u_{n,m-1} + u_{n,m+1}) \\ - k_{c_x}(u_{n-a,m} - u_{n-(a+1),m}) - k_{c_y}(u_{n,m-a} - u_{n,m-(a+1)}) = 0. \end{aligned} \tag{5}$$

3.1. Dispersion relations, non-reciprocity and directionality

We impose Bloch wave solutions in equation (4) of the form $u_{n,m} = Ue^{i(\omega t - \mu_x n - \mu_y m)}$, where μ_x and μ_y are the wave vector components along x and y, respectively. This gives:

$$\Omega^2 = 2(2 - \cos\mu_x - \cos\mu_y) - \gamma_x e^{i\mu_x a}(1 - e^{i\mu_x}) - \gamma_y e^{i\mu_y a}(1 - e^{i\mu_y}), \tag{6}$$

where again $\Omega = \omega/\omega_0$, with $\omega_0 = \sqrt{k/m}$, while $\gamma_x = k_{c_x}/k$ and $\gamma_y = k_{c_y}/k$. Similar to the 1D case, we consider the solution with $\Omega_r > 0$ to describe dispersion, such that $\Omega_i < 0$ is associated with wave amplification, while $\Omega_i > 0$ with attenuation.

For local control ($a = 0$), figures 8(a) and (b) display the real and imaginary iso-frequency contours of the dispersion surfaces of a lattice with $\gamma_x = \gamma_y = 0.1$. While the real part (figure 8(a)) closely resembles that of a passive 2D lattice [2], the imaginary part of the frequency contours (figure 8(b)) exhibits directional dependent attenuation and amplification zones. In particular, a region for which $\Omega_i < 0$ is identified in the third quadrant of the μ_x, μ_y plane (figure 8(b)), revealing a range of directions of wave amplification. This is further illustrated by considering the contour for $\Omega = 0.7$, highlighted by the thick black line in figure 8(a), which is approximately circular, possibly suggesting isotropic propagation. However, the wave vector components at this frequency (also highlighted by the thick black circle in figure 8(b)), cross regions of positive and negative imaginary frequency. The angular dependence of Ω_i is shown in figure 8(d), where it is plotted in polar form versus the propagation angle $\theta = \tan^{-1}(\mu_y/\mu_x)$. In the figure, the thick blue lobe denotes amplification for $\Omega_i < 0$, while the thin red line defines the angular range associated with attenuation. Maximum amplification is found for $\theta \approx 225^\circ$, which corresponds to waves traveling towards the left bottom corner of a square lattice. Transient time domain simulations are conducted on a lattice with 100×100 masses, with forcing consisting of a 5-cycle sinusoidal burst of frequency $\Omega = 0.7$ (similar to that of figures 2(e) and (f)) applied to the center mass of the lattice. The response is evaluated by numerical integration of the equations of motion (equation (2)), similar to the procedure applied to the study of 1D lattices, where the global mass and stiffness matrices **M** and **K** are

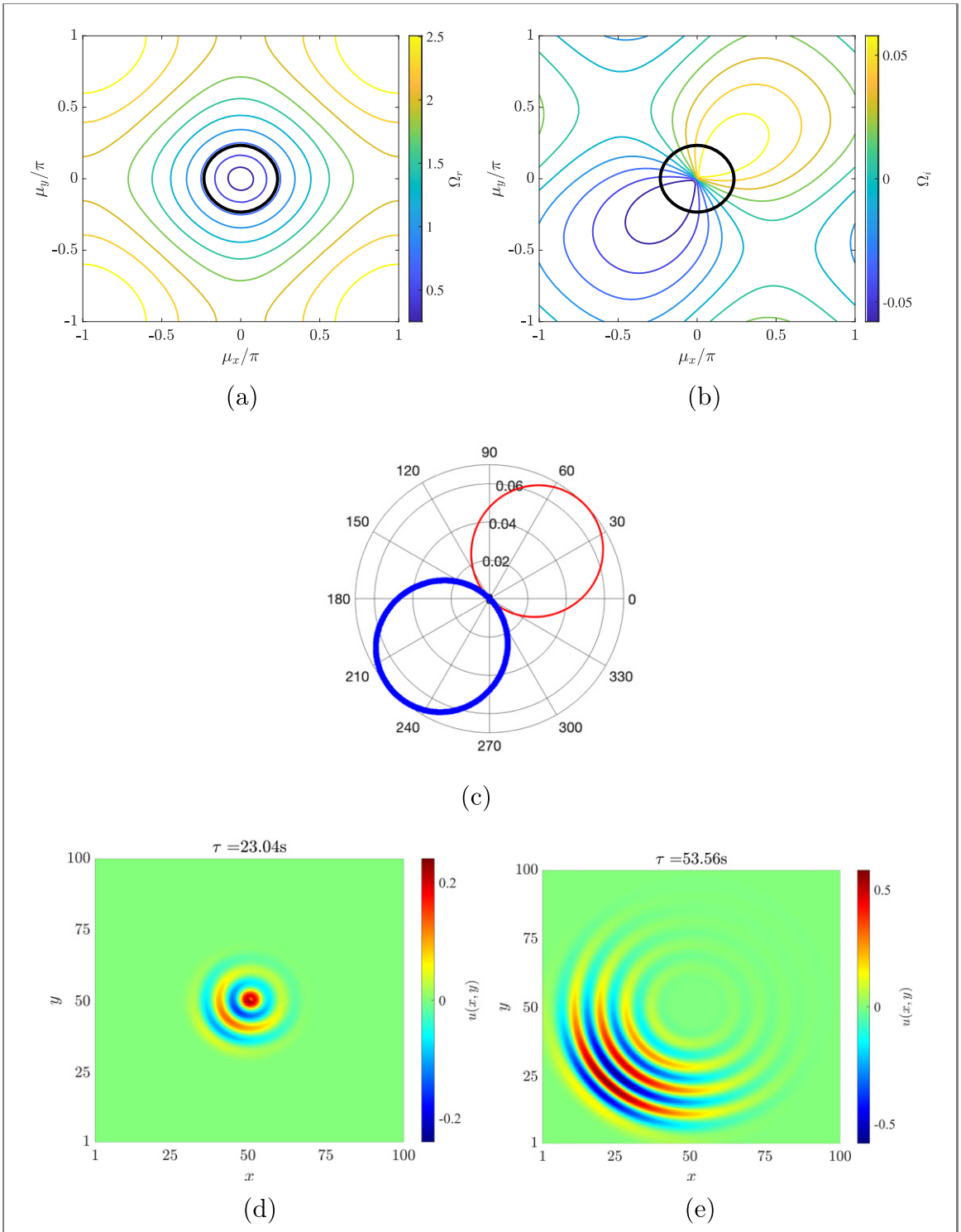

Figure 8. Non-reciprocal amplification and attenuation of waves in 2D lattice with feedback parameters $a = 0$, $\gamma_x = \gamma_y = 0.1$. Iso-frequency contours corresponding to the real part Ω_r (a), and imaginary part Ω_i (b) of the dispersion $\Omega(\mu_x, \mu_y)$. The thick black line outlines the contour for $\Omega_r = 0.7$, and defines the wave vector components pairs μ_x, μ_y governing propagation at the considered frequency. Angular variation of Ω_i highlighting the angular range of amplification (thick blue line) and attenuation (thin red line) (c). Snapshots of transient response to a tone-burst excitation at $\Omega = 0.7$ applied to the center mass of the lattice illustrating that waves traveling towards the bottom left corner are preferentially amplified (d, e).

assembled for the 2D lattice using equation (4). Snapshots of the lattice motion at two subsequent time instants displayed in figures 8(d) and (e) confirm that waves are preferentially amplified as they travel towards the bottom left corner of the lattice.

The direction of preferential amplification can be tuned based on the feedback parameters γ_x, γ_y, as illustrated in figure 9, again for $\Omega = 0.7$. Letting $\gamma_x = 0.1$ and varying γ_y changes the direction of preferential amplification, as illustrated for 3 representative γ_y values (0.07, 0.03 and 0) in the imaginary dispersion components polar plots of figures 9(a)–(c). Snapshots of the transient response in

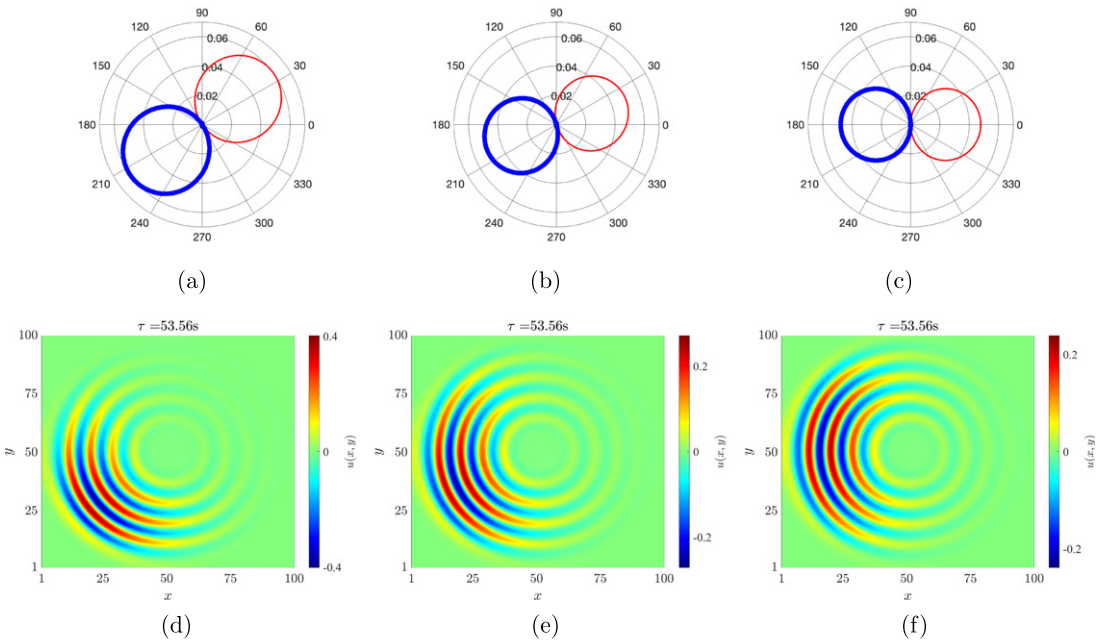

Figure 9. Tunability of non-reciprocal wave amplification in 2D lattices with feedback interactions ($a = 0$, $\gamma_x = 0.1$) for $\Omega_r = 0.7$. Polar plots of the imaginary component of the dispersion showing angular ranges of amplification (thick blue line) and attenuation (thin red line) displayed for $\gamma_y = 0.07$ (a), $\gamma_y = 0.03$ (b), and $\gamma_y = 0$ (c) demonstrate a transition of the preferential wave amplification direction based on feedback control. Snapshots of transient response to a sine-burst excitation of center frequency $\Omega = 0.7$ are displayed in (d) and (e), illustrating the change in the directions of amplification for each case.

figures 9(d) and (e) confirm that waves are preferentially amplified according to the predicted directions. Other combinations of γ_x, γ_y can tune the direction of amplification, suggesting that anisotropy in the control laws ($\gamma_x \neq \gamma_y$) can be employed for non-reciprocal directional amplification, which may significantly expand the functionality of reciprocal directionality encountered in passive 2D lattices with anisotropy in spring constants [2].

Similar to the 1D case, non-local feedback interactions in 2D lattices produce multiple non-reciprocal bands. This is illustrated for a lattice with $a = 1$ and $\gamma_x = \gamma_y = 0.3$ in figure 10. The real part of the dispersion displayed in figure 10(a) is similar to that of the local case (figure 8(a)). In contrast, the imaginary component of the dispersion (figure 10(b)) exhibits different regions of amplification and attenuation when compared to the local case (figure 8(b)). Contours at three different Ω_r values are highlighted in figure 10(a): $\Omega_r = 0.5$–black circles, $\Omega_r = 1.75$–black dashed line, and $\Omega_r = 2.5$–black solid line. The corresponding wave vector component pairs are also displayed in figure 10(b), while angular variations of the amplification (thick blue line), and attenuation (red thin line) at these frequencies are shown in figures 10(c)–(e): wave amplification occurs along different, and opposite directions within the range of frequencies defined by the dispersion relation of the lattice. Such behavior is confirmed by evaluating the transient response to a broad-band input (figures 3(e) and (f)) applied to the center mass of the lattice. Two subsequent snapshots of the lattice motion (figures 10(f) and (g)), illustrate how the broadband input is decomposed into approximately 4 wave packets that propagate along the distinct directions predicted by the imaginary component of dispersion.

3.2. Bulk topology, skin modes and corner modes

We extend the winding number analysis conducted for 1D lattices to describe the topological properties of 2D lattices and demonstrate the presence of skin edge and corner modes. We illustrate that the dispersion for a finite lattice is associated with modes localized at one of the boundaries, that are either amplified or attenuated as they propagate along the other (infinite) direction. We then show that the combined effect of localization for finite strips in two directions (x and y) produce modes that are localized at the corners of finite lattices.

As a representative case, we consider a finite strip of $N = 30$ masses along the x direction, and infinite along the y direction, with parameters $a = 1$, $\gamma_x = \gamma_y = 0.3$ (corresponding to the lattice described in figure 10). The dispersion of the finite lattice strip is computed by solving an Eigenvalue problem of the form $\mathbf{K}(\mu_y)\boldsymbol{u} = \omega^2\mathbf{M}\boldsymbol{u}$ for distinct values of μ_y, where the stiffness matrix $\mathbf{K}(\mu_y)$ is assembled by using equation (4) with the assumption of waves traveling along y only, i.e. $u_{n,m} = u_n e^{i(\omega t - \mu_y m)}$, and with free–free

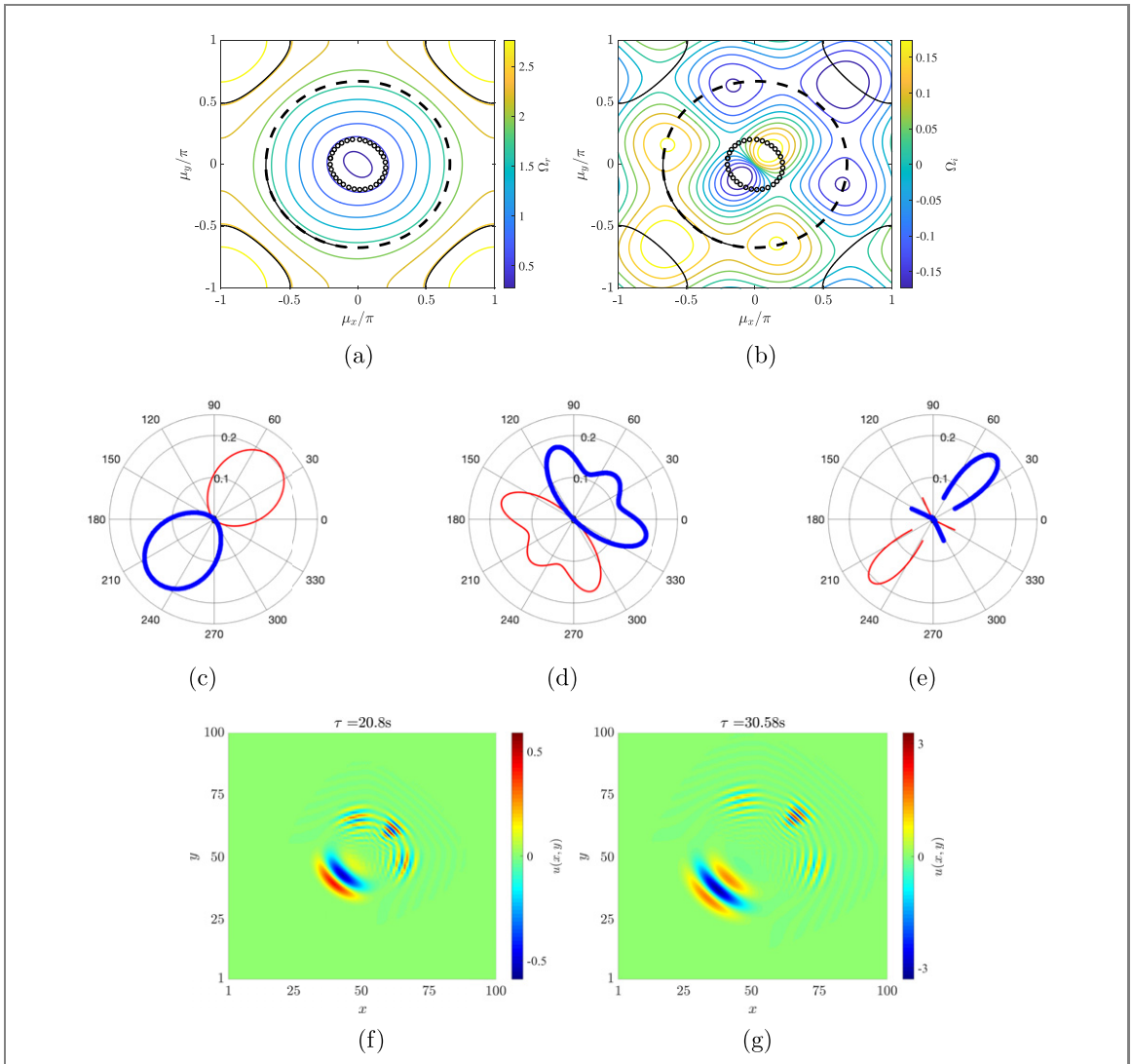

Figure 10. Non-reciprocal wave amplification for 2D lattices with non-local feedback interactions ($a = 1, \gamma_x = \gamma_y = 0.3$). Real (a) and imaginary (b) components of the dispersion are displayed along with contours associated with $\Omega_r = 0.5$–black circles, $\Omega_r = 1.75$–black dashed line, and $\Omega_r = 2.5$ black solid line. Corresponding polar plots of the imaginary frequency components showing angular ranges of angular amplification (thick blue line), and attenuation (red thin line) (c)–(e): the non-locality of the feedback interactions result in multiple frequency/wavenumber bands where waves are amplified towards different directions. The behavior predicted by the dispersion analysis is illustrated by snapshots representing the lattice response to a broadband input (figures 3(e) and (f)) at subsequent time instants (f, g).

boundary conditions in x. The dispersion for $\mu_y = -\pi$, i.e. $\Omega(\mu_x, \mu_y = -\pi)$ is shown in figure 11(a): its projection on the complex plane defines a loop represented by red lines in figure 11(b). The Eigen frequencies of the finite strip for $\mu_y = -\pi$ are represented by dots in figure 11(b), while a few representative modes marked by blue circles in figure 11(b) have their mode shapes displayed in figure 11(c), revealing localization at the boundaries. The localization of the strip modes for a given μ_y is related to the topology of the dispersion $\Omega(\mu_x)$ at that μ_y value. Hence, the winding number ν for a given μ_y is computed through equation (3) with integration in μ_x

$$\nu = \frac{1}{2\pi \mathrm{i}} \int_{-\pi}^{\pi} \frac{\Omega'}{\Omega - \Omega_b} \mathrm{d}\mu_x, \tag{7}$$

with $\Omega' = \partial\Omega/\partial\mu_x$. In figure 11(b), blue and red zones again define regions for which $\nu = -1$ and $\nu = 1$, and similar to the 1D lattices, modes of the finite strip whose Eigen frequencies lie inside such regions are respectively localized at the left (blue dots) or right (red dots) boundary (figure 11(c)). One particular mode marked by the black dot lies on top of the left end of the dispersion loop, and is characterized by displacements of all masses uniform along x due to the free-free boundaries. Repeating this procedure for $\mu_y \in [-\pi, \pi]$ leads to the complete characterization of the finite strip dispersion (figure 11(d)): blue and red areas represent regions with bulk invariants $\nu = -1$ and $\nu = 1$ (the dispersion loops are not shown for better visualization), hence modes of the finite strip spanning such regions are localized at the left (blue dots) or right (red dots) boundary. The real and imaginary components of the finite strip dispersion are

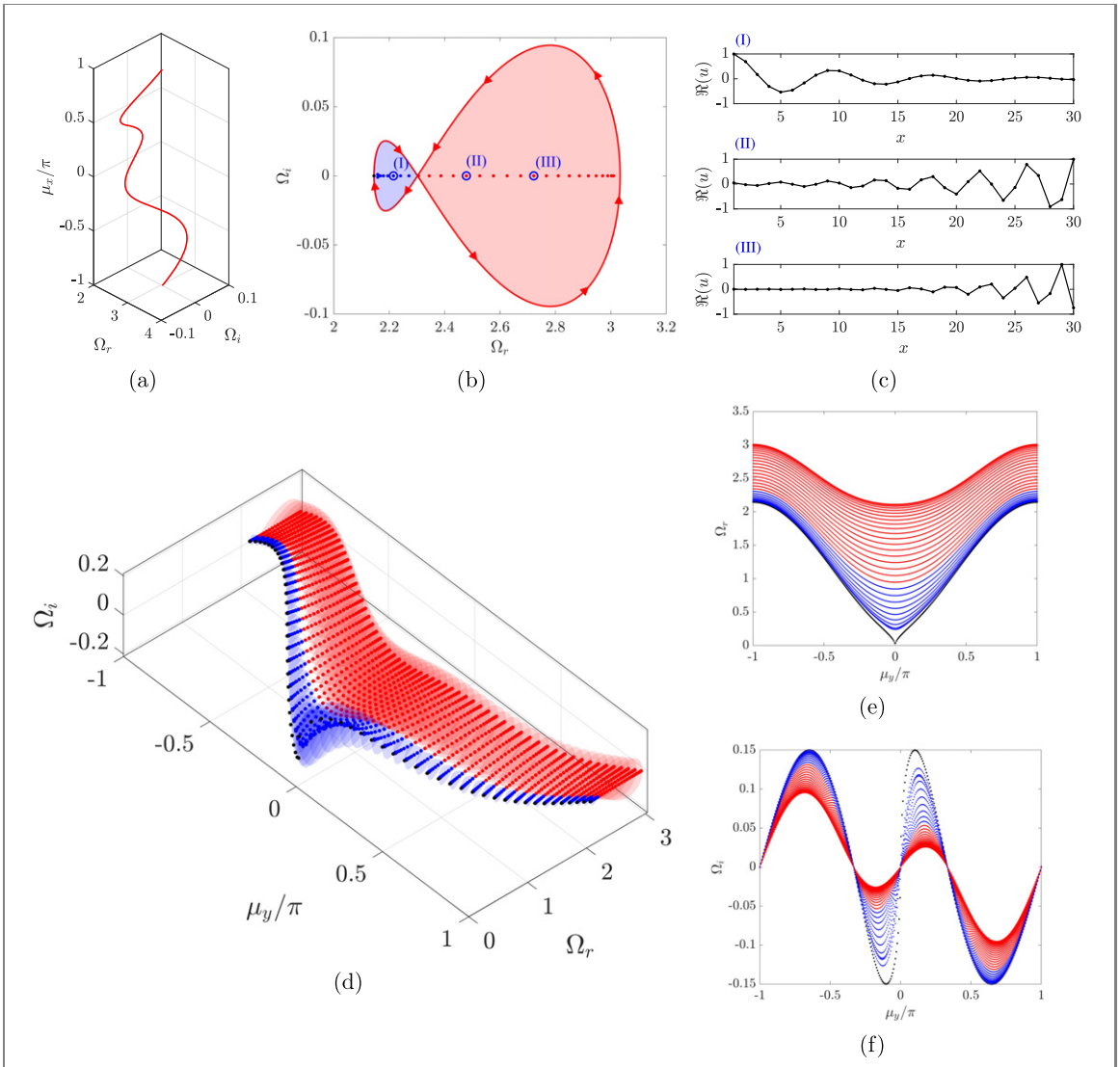

Figure 11. Bulk topology and skin modes of finite strip with $N = 30$ masses along x for lattice with feedback parameters $a = 1$, $\gamma_x = \gamma_y = 0.3$. The dispersion $\Omega(\mu_x, \mu_y = -\pi)$ (a) defines a closed loop on the complex plane (red lines in (b)), identifying two regions with winding numbers $\nu = -1$ (blue) and $\nu = 1$ (red). Modes of the finite strip for $\mu_y = -\pi$ are localized at the left or right boundary (c) when their Eigen frequencies lie inside regions with $\nu = -1$ (blue dots) or $\nu = 1$ (red dots), respectively. The procedure repeated for $\mu_y \in \{-\pi, \pi\}$ results in a representation of the bulk topology as red and blue regions representing different winding numbers, and modes of the finite strip spanning such regions are therefore localized at the left (blue dots) or right (red dots) boundary. The real and imaginary frequency components of the finite strip dispersion are displayed in (e, f) revealing non-reciprocity in amplification/attenuation of the localized modes propagating along the y direction.

separately displayed in figures 11(e) and (f), revealing that the each mode exhibits non-reciprocity, similarly to 1D lattices with $a = 1$ (figure 3(a)). This opens the possibility of establishing non-reciprocal wave amplification as demonstrated in figure 3 at the edges of a 2D lattice.

The same procedure applied to the finite strip along x can be repeated for a finite strip with $N = 30$ masses along y instead, and infinite along the x direction. In line with recent work in quantum lattices [74], we find that the combined effect of the localized strip modes for the x and y directions lead to the localization of modes at one or more corners. Illustrative corner modes for a 30×30 lattice are displayed in figure 12. The localization at these corners is also in line with the non-reciprocal wave amplification behavior reported in figure 10, where wave amplification occurs either towards the bottom left corner, upper right corner, or simultaneously towards the upper left corner and bottom right corner. Although winding numbers of the dispersion bands can be used to predict the localization of strip modes (finite along one direction but infinite along the other), to the authors knowledge they cannot be directly used to predict the regions where modes of finite 2D lattices are localized, based solely on where their frequency lies in the complex plane. We interpret their localization to occur due to a superposition of the effects leading to the localization of the strip modes in both directions [74]. However, additional investigations are necessary to

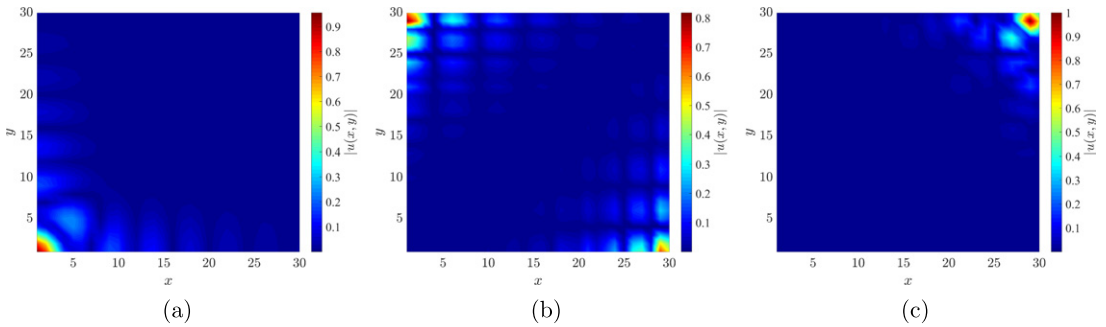

Figure 12. Representative modes localized at corners of finite 2D lattice with 30×30 masses and feedback parameters $a = 1$, $\gamma_x = \gamma_y = 0.3$. The localization occurs due to the combined effect of localized skin modes for both the x and y directions.

identify a procedure that predicts regions of localization based on topological invariants such as winding numbers.

4. Conclusions

We investigate a family of elastic lattices where non-local feedback interactions lead to a series of unconventional *phenomena* associated with the physics of non-Hermitian systems. Among the key results, we demonstrate non-reciprocity associated with attenuation and amplification for waves propagating in different directions in 1D and 2D lattices, along with their topological properties associated with winding number of the complex dispersion bands, and localization of bulk modes at edges and corners. While idealized spring-mass lattices where used herein to elucidate the fundamental properties of elastic media with feedback interactions, we highlight that already existing platforms used to experimentally realize active materials with time-modulated properties [32–36] may potentially be modified to support feedback interactions of the type introduced here. The presented results open new possibilities for the design of active meta materials with novel functionalities such as those related to selective wave filtering, splitting, amplification and localization, both in one and two dimensions. Our results also corroborate recent observations [45, 46] that feedback control may be a fruitful strategy to investigate the physics and topology of non-Hermitian systems. While this work focuses on single-banded systems (already exhibiting a series of interesting properties), multiple possibilities are open for future work, such as exploring lattices with different geometries, modulations of control parameters and/or modification of control laws (e.g. derivative and integral controls), as well as the introduction of non-linearities.

Acknowledgments

The authors gratefully acknowledge the support from the National Science Foundation (NSF) through the EFRI 1741685 Grant and from the Army Research office through Grant W911NF-18-1-0036.

Appendix. Non-Hermitian skin effect under different boundary conditions

The non-Hermitian skin effect (NSHE) manifests as modes localized at the boundaries of finite lattices, whose localization edge can be predicted based on the winding number of the complex dispersion bands. In the manuscript, numerous examples were presented for lattices with free–free boundary conditions. The NHSE can also be observed under different boundary conditions, such as fixed–fixed or fixed–free, as illustrated in this appendix. Figures A1(a) and (c) show the complex dispersion loops (red lines) for the lattice with $a = 3, \gamma_c = 0.1$, which are the same as figure 5(e). Eigen frequencies for a finite lattice with $N = 100$ masses and fixed-free boundary conditions ($u_1 = 0$) are displayed as black dots in figure A1(a), while figure A1(c) exhibits Eigen frequencies for the fixed-fixed case ($u_1, u_N = 0$). While the frequencies are generally distinct, the corresponding modes are localized at either the left or right boundary when Eigen frequencies lie in regions with $\nu = -1$ and $\nu = 1$, respectively. Selected modes highlighted by blue circles in figures A1(a) and (c) have their mode shape displayed in figures A1(b) and (d), illustrating the persistence of the NHSE, predicted by the winding number of the dispersion loops, for different boundary conditions.

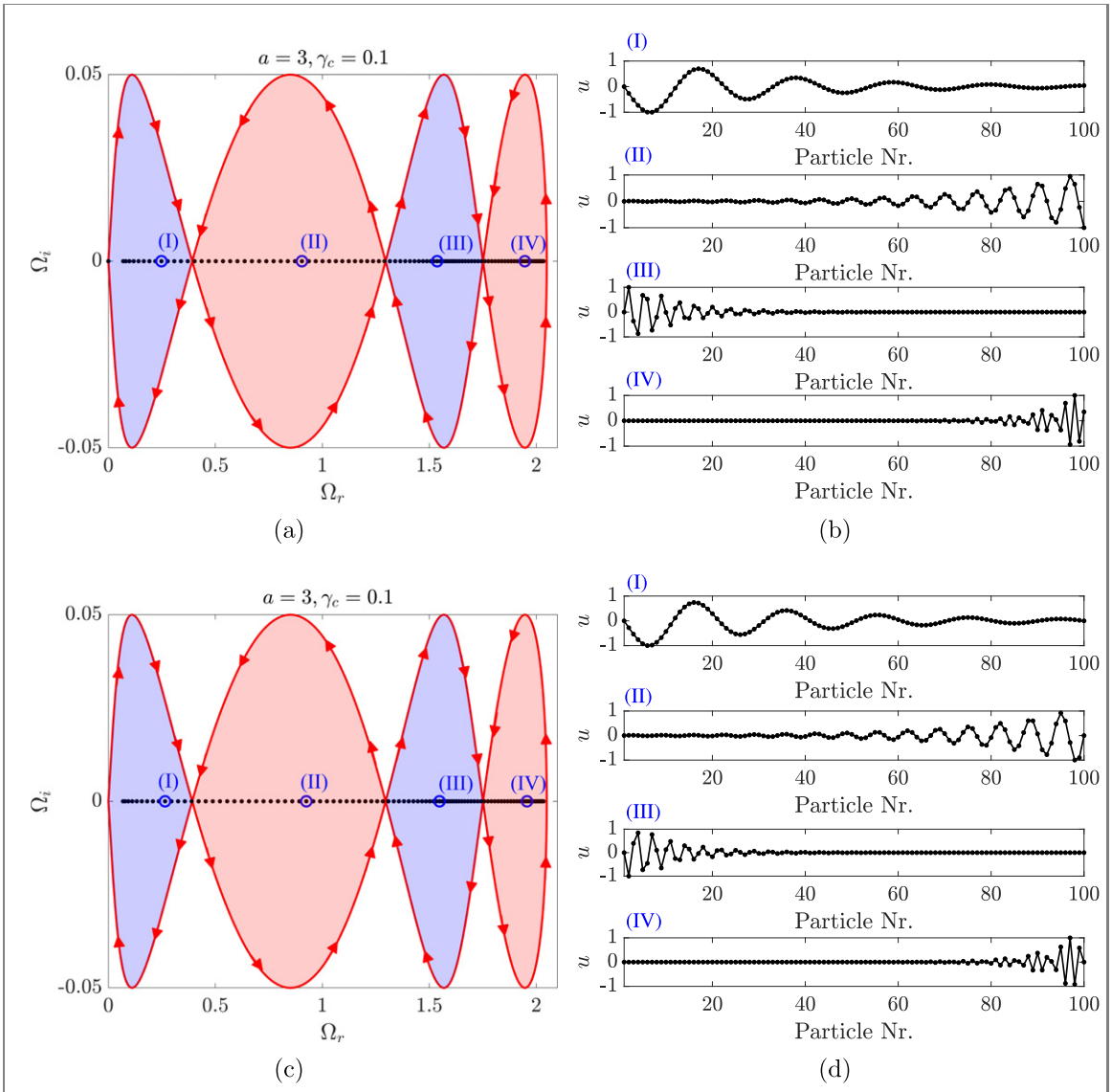

Figure A1. Non-Hermitian skin effect under different boundary conditions for lattice with $a = 3, \gamma_c = 0.1$. The complex dispersion loops (red lines) displayed in (a, c) identify the phases associated with different winding numbers $\nu = -1$ (blue) and $\nu = 1$ (red). Eigen frequencies for a finite lattice with $N = 100$ and fixed-free boundary conditions ($u_1 = 0$) are displayed as black dots in (a), while the fixed–fixed case ($u_1 = u_N = 0$) is exhibited in (c). For both cases, the modes of the finite lattice (b, d) are localized at either the left of right boundary when their Eigen frequencies lie in regions with winding number $\nu = -1$ and $\nu = 1$, respectively.

Reference

[1] Lu M-H, Liang F and Chen Y-F 2009 Phononic crystals and acoustic meta materials *Mater. Today* **12** 34–42
[2] Hussein M I, Leamy M J and Ruzzene M 2014 Dynamics of phononic materials and structures: historical origins, recent progress, and future outlook *Appl. Mech. Rev.* **66** 040802
[3] Huang H H and Sun C T 2009 Wave attenuation mechanism in an acoustic meta material with negative effective mass density *New J. Phys.* **11** 013003
[4] Yang Z, Dai H M, Chan N H, Ma G C and Sheng P 2010 Acoustic meta material panels for sound attenuation in the 50–1000 hz regime *Appl. Phys. Lett.* **96** 041906
[5] Steven Lin S-C, Huang T J, Sun J-H and Wu T-T 2009 Gradient-index phononic crystals *Phys. Rev.* B **79** 094302
[6] Cummer S A and Schurig D 2007 One path to acoustic cloaking *New J. Phys.* **9** 45
[7] Miniaci M, Krushynska A, Bosia F and Pugno N M 2016 Large scale mechanical meta materials as seismic shields *New J. Phys.* **18** 083041
[8] Hasan M Z and Kane C L 2010 Colloquium: topological insulators *Rev. Mod. Phys.* **82** 3045
[9] Lu L, Joannopoulos J D and Soljačić M 2014 Topological photonics *Nat. Photon.* **8** 821
[10] Huber S D 2016 Topological mechanics *Nat. Phys.* **12** 621
[11] Yang Z, Gao F, Shi X, Lin X, Gao Z, Chong Y and Zhang B 2015 Topological acoustics *Phys. Rev. Lett.* **114** 114301
[12] Ma G, Xiao M and Chan C T 2019 Topological phases in acoustic and mechanical systems *Nat. Rev. Phys.* **1** 281–94
[13] Fleury R, Khanikaev A B and Alu A 2016 Floquet topological insulators for sound *Nat. Commun.* **7** 11744
[14] Hossein Mousavi S, Khanikaev A B and Wang Z 2015 Topologically protected elastic waves in phononic meta materials *Nat. Commun.* **6** 8682

[15] Roman S and Huber S D 2015 Observation of phononic helical edge states in a mechanical topological insulator *Science* **349** 47–50
[16] Wang P, Lu L and Bertoldi K 2015 Topological phononic crystals with one-way elastic edge waves *Phys. Rev. Lett.* **115** 104302
[17] Nash L M, Kleckner D, Read A, Vitelli V, Turner A M and Irvine W T M 2015 Topological mechanics of gyroscopic meta materials *Proc. Natl Acad. Sci.* **112** 14495–500
[18] Pal R K and Ruzzene M 2017 Edge waves in plates with resonators: an elastic analogue of the quantum valley hall effect *New J. Phys.* **19** 025001
[19] Miniaci M, Pal R K, Morvan B and Ruzzene M 2018 Experimental observation of topologically protected helical edge modes in patterned elastic plates *Phys. Rev.* X **8** 031074
[20] Liu T-W and Semperlotti F 2018 Tunable acoustic valley–hall edge states in reconfigurable phononic elastic waveguides *Phys. Rev. Appl.* **9** 014001
[21] Chaunsali R, Chen C-W and Yang J 2018 Sub wavelength and directional control of flexural waves in zone-folding induced topological plates *Phys. Rev.* B **97** 054307
[22] IN Rosa M, Pal R K, Arruda J R F and Ruzzene M 2019 Edge states and topological pumping in spatially modulated elastic lattices *Phys. Rev. Lett.* **123** 034301
[23] Hotzen Grinberg I, Lin M, Harris C, Benalcazar W A, Peterson C W, Hughes T L and Bahl G 2020 Robust temporal pumping in a magneto-mechanical topological insulator *Nat. Commun.* **11** 974
[24] Chen H, Yao L Y, Nassar H and Huang G L 2019 Mechanical quantum hall effect in time-modulated elastic materials *Phys. Rev. Appl.* **11** 044029
[25] Riva E, IN Rosa M and Ruzzene M 2019 Edge states and topological pumping in stiffness modulated elastic plates (arXiv:1911.02567)
[26] Brouzos I, Kiorpelidis I, Diakonos F K and Theocharis G 2019 Non-adiabatic time-optimal edge mode transfer on mechanical topological chain (arXiv:1911.03375)
[27] Apigo D J, Cheng W, Dobiszewski K F, Prodan E and Prodan C 2019 Observation of topological edge modes in a quasi periodic acoustic waveguide *Phys. Rev. Lett.* **122** 095501
[28] Ni X, Chen K, Weiner M, Apigo D J, Prodan C, Andrea A, Prodan E and Khanikaev A B 2019 Observation of hofstadter butterfly and topological edge states in reconfigurable quasi-periodic acoustic crystals *Commun. Phys.* **2** 55
[29] Pal R K, Rosa M I N and Ruzzene M 2019 Topological bands and localized vibration modes in quasi periodic beams *New J. Phys.* **21** 093017
[30] Fleury R, Sounas D L, Sieck C F, Haberman M R and Andrea A 2014 Sound isolation and giant linear nonreciprocity in a compact acoustic circulator *Science* **343** 516–9
[31] Trainiti G and Ruzzene M 2016 Non-reciprocal elastic wave propagation in spatiotemporal periodic structures *New J. Phys.* **18** 083047
[32] Wang Y, Yousefzadeh B, Chen H, Nassar H, Huang G and Daraio C 2018 Observation of nonreciprocal wave propagation in a dynamic phononic lattice *Phys. Rev. Lett.* **121** 194301
[33] Chen Y, Li X, Nassar H, Norris A N, Daraio C and Huang G 2019 Nonreciprocal wave propagation in a continuum-based meta material with space-time modulated resonators *Phys. Rev. Appl.* **11** 064052
[34] Marconi J, Riva E, Di Ronco M, Cazzulani G, Braghin F and Ruzzene M 2019 Experimental observation of non-reciprocal band-gaps in a space-time modulated beam using a shunted piezoelectric array (arXiv:1909.13224)
[35] Karkar S, De Bono E, Collet M, Matten G, Ouisse M and Rivet E 2019 Broadband nonreciprocal acoustic propagation using programmable boundary conditions: from analytical modeling to experimental implementation *Phys. Rev. Appl.* **12** 054033
[36] MA A, Callanan J and Nouh M 2020 Experimental observation of nonreciprocal waves in a resonant meta material beam *Phys. Rev. Appl.* **13** 021001
[37] Coulais C, Sounas D and Andrea A 2017 Static non-reciprocity in mechanical meta materials *Nature* **542** 461
[38] Bunyan J, Moore K J, Mojahed A, Fronk M D, Leamy M, Tawfick S and Vakakis A F 2018 Acoustic non reciprocity in a lattice incorporating nonlinearity, asymmetry, and internal scale hierarchy: experimental study *Phys. Rev.* E **97** 052211
[39] Darabi A, Fang L, Mojahed A, Fronk M D, Vakakis A F and Leamy M J 2019 Broadband passive nonlinear acoustic diode *Phys. Rev.* B **99** 214305
[40] Mojahed A, Bunyan J, Tawfick S and Vakakis A F 2019 Tunable acoustic non reciprocity in strongly nonlinear waveguides with asymmetry *Phys. Rev. Appl.* **12** 034033
[41] Konstantinos G M, El-Ganainy R, Christodoulides D N and Musslimani Z H 2008 Beam dynamics in p t symmetric optical lattices *Phys. Rev. Lett.* **100** 103904
[42] Han Z, Qiao X, Wu T, Midya B, Longhi S and Liang F 2019 Non-hermitian topological light steering *Science* **365** 1163–6
[43] Xu H, Mason D, Jiang L and Harris J G E 2016 Topological energy transfer in an opto mechanical system with exceptional points *Nature* **537** 80
[44] Fleury R, Sounas D and Alu A 2015 An invisible acoustic sensor based on parity-time symmetry *Nat. Commun.* **6** 5905
[45] Ghatak A, Brandenbourger M, van Wezel J and Coulais C 2019 Observation of non-hermitian topology and its bulk-edge correspondence (arXiv:1907.11619)
[46] Brandenbourger M, Locsin X, Lerner E and Coulais C 2019 Non-reciprocal Robotic Meta materials (arXiv:1903.03807)
[47] Bender C M and Boettcher S 1998 Real spectra in non-hermitian hamiltonians having p t symmetry *Phys. Rev. Lett.* **80** 5243
[48] Longhi S 2018 Parity-time symmetry meets photonics: a new twist in non-hermitian optics *Europhys. Lett.* **120** 64001
[49] El-Ganainy R, Makris K G, Khajavikhan M, Musslimani Z H, Rotter S and Christodoulides D N 2018 Non-hermitian physics and pt symmetry *Nat. Phys.* **14** 11–9
[50] Miri M-A and Andrea A 2019 Exceptional points in optics and photonics *Science* **363** eaar7709
[51] Lin Z, Ramezani H, Eichelkraut T, Kottos T, Cao H and Christodoulides D N 2011 Unidirectional invisibility induced by p t-symmetric periodic structures *Phys. Rev. Lett.* **106** 213901
[52] Liang F, Wong Z J, Ma R-M, Wang Y and Zhang X 2014 Single-mode laser by parity-time symmetry breaking *Science* **346** 972–5
[53] Hodaei H, Hassan U A, Wittek S, Garcia-Gracia H, El-Ganainy R, Christodoulides D N and Khajavikhan M 2017 Enhanced sensitivity at higher-order exceptional points *Nature* **548** 187
[54] Chen W, Kaya Özdemir , Zhao G, Jan W and Yang L 2017 Exceptional points enhance sensing in an optical micro cavity *Nature* **548** 192
[55] Gong Z, Ashida Y, Kawabata K, Takasan K, Higashikawa S and Ueda M 2018 Topological phases of non-hermitian systems *Phys. Rev.* X **8** 031079

[56] Shen H, Zhen B and Fu L 2018 Topological band theory for non-hermitian hamiltonians *Phys. Rev. Lett.* **120** 146402
[57] Ghatak A and Das T 2019 New topological invariants in non-hermitian systems *J. Phys.: Condens. Matter.* **31** 263001
[58] Torres L EF F 2019 Perspective on topological states of non-hermitian lattices *J. Phys. Mater.* **3** 014002
[59] Bergholtz E J, Budich J C and Kunst F K 2019 Exceptional topology of non-hermitian systems (arXiv:1912.10048)
[60] Xu Y, Wang S-T and Duan L-M 2017 Weyl exceptional rings in a three-dimensional dissipative cold atomic gas *Phys. Rev. Lett.* **118** 045701
[61] Zhou H, Peng C, Yoon Y, Hsu C W, Nelson K A, Fu L, Joannopoulos J D, Soljačić M and Zhen B 2018 Observation of bulk fermi arc and polarization half charge from paired exceptional points *Science* **359** 1009–12
[62] E Lee T 2016 Anomalous edge state in a non-hermitian lattice *Phys. Rev. Lett.* **116** 133903
[63] Xiong Y 2018 Why does bulk boundary correspondence fail in some non-hermitian topological models *J. Phys. Commun.* **2** 035043
[64] Kawabata K, Shiozaki K, Ueda M and Sato M 2019 Symmetry and topology in non-hermitian physics *Phys. Rev.* X **9** 041015
[65] Yao S and Wang Z 2018 Edge states and topological invariants of non-hermitian systems *Phys. Rev. Lett.* **121** 086803
[66] Martinez Alvarez V M, Vargas JE B and Torres L EF F 2018 Non-hermitian robust edge states in one dimension: anomalous localization and Eigen space condensation at exceptional points *Phys. Rev.* B **97** 121401
[67] Kunst F K, Edvardsson E, Budich J C and Bergholtz E J 2018 Bi orthogonal bulk-boundary correspondence in non-hermitian systems *Phys. Rev. Lett.* **121** 026808
[68] Lee C H and Thomale R 2019 Anatomy of skin modes and topology in non-hermitian systems *Phys. Rev.* B **99** 201103
[69] Longhi S 2019 Probing non-hermitian skin effect and non-bloch phase transitions *Phys. Rev. Res.* **1** 023013
[70] Yoshida T, Mizoguchi T and Hatsugai Y 2019 Mirror skin effect and its electric circuit simulation (arXiv:1912.12022)
[71] Borgnia D S, Kruchkov A J and Slager R-J 2019 Non-hermitian boundary modes (arXiv:1902.07217)
[72] Hofmann T *et al* 2019 Reciprocal skin effect and its realization in a topo electrical circuit (arXiv:1908.02759)
[73] Xiao L, Deng T, Wang K, Zhu G, Wang Z, Yi W and Xue P 2019 Observation of non-hermitian bulk-boundary correspondence in quantum dynamics (arXiv:1907.12566)
[74] Lee C H, Li L and Gong J 2019 Hybrid higher-order skin-topological modes in nonreciprocal systems *Phys. Rev. Lett.* **123** 016805
[75] Liu T, Zhang Y-R, Qing A, Gong Z, Kawabata K, Ueda M and Nori F 2019 Second-order topological phases in non-hermitian systems *Phys. Rev. Lett.* **122** 076801
[76] Zhu X, Ramezani H, Shi C, Zhu J and Zhang X 2014 P t-symmetric acoustics *Phys. Rev.* X **4** 031042
[77] Christensen J, Willatzen M, Velasco V R and Lu M-H 2016 Parity-time synthetic phononic media *Phys. Rev. Lett.* **116** 207601
[78] Liu T, Zhu X, Chen F, Liang S and Zhu J 2018 Unidirectional wave vector manipulation in two-dimensional space with an all passive acoustic parity-time-symmetric meta materials crystal *Phys. Rev. Lett.* **120** 124502
[79] Zhang Z, Rosendo López M, Cheng Y, Liu X and Christensen J 2019 Non-hermitian sonic second-order topological insulator *Phys. Rev. Lett.* **122** 195501
[80] Rosendo López M, Zhang Z, Torrent D and Christensen J 2019 Multiple scattering theory of non-hermitian sonic second-order topological insulators *Commun. Phys.* **2** 132
[81] Wu Q, Chen Y and Huang G 2019 Asymmetric scattering of flexural waves in a parity-time symmetric metamaterial beam *J. Acoust. Soc. Am.* **146** 850–62
[82] Hou Z and Assouar B 2018 Tunable elastic parity-time symmetric structure based on the shunted piezoelectric materials *J. Appl. Phys.* **123** 085101
[83] Ahlfers L V 1966 *Complex Analysis; an Introduction to the Theory of Analytic Functions of One Complex Variable*